

Evaluation of HCF Multiaxial Fatigue Life Prediction Methodologies for Ti-6Al-4V

Mr. Ahmo Krgo and Dr. Alan R. Kallmeyer
Graduate Research Assistant and Assistant Professor, respectively
Department of Mechanical Engineering
North Dakota State University, Fargo, ND 58105

Dr. Peter Kurath
Adj. Associate Professor
Department of Mechanical Engineering
University of Illinois at Urbana-Champaign, Urbana, IL 61801

INTRODUCTION

In recent years, interpretation of the damage mechanisms associated with fatigue loading has led to the development of improved fatigue damage parameters and relatively reliable methods for modeling the nucleation and progression of fatigue cracks. Historically, the majority of fatigue research has been directed towards problems involving uniaxial stress states. However, many critical engineering components, such as crankshafts, axles, turbine blades, and notched components, are routinely subjected to cyclic multiaxial stress states. In many cases the loading is non-proportional or may involve multidimensional mean stresses. The successful design of such components requires that appropriate damage algorithms for multiaxial stress states be identified for fatigue life prediction.

Although numerous multiaxial fatigue models have been proposed in the technical literature, most of these are based on experiments performed on common steel and aluminum alloys in the low cycle fatigue regime. With the increasing use of advanced metals in applications where high cycle fatigue (HCF) conditions prevail, there is a pressing need to identify or develop multiaxial fatigue models capable of predicting the long-term behavior of such materials. The objective of this research is to identify reliable multiaxial fatigue models that can be used for HCF life prediction of advanced monolithic engine and airframe materials. In this paper, existing multiaxial fatigue models, including both equivalent-stress and critical-plane approaches, are evaluated to determine their capabilities when applied to Ti-6Al-4V under multiaxial HCF loading. As part of this effort, biaxial (tension/torsion) fatigue tests were conducted on smooth specimens of Ti-6Al-4V, which included non-proportional loading cases. The multiaxial fatigue models were evaluated based on their ability to correlate the biaxial data with uniaxial fatigue data, at various R ratios, for this material. The influence of mean stresses in multiaxial fatigue is also addressed.

EXPERIMENTAL PROCEDURES AND RESULTS

The biaxial test specimens were machined from 20 mm thick, forged Ti-6Al-4V plates. After machining, the specimens were stress relieved and chem milled to eliminate residual stresses and surface damage. Solid specimens with a grip diameter of approximately 19 mm, and a gage section diameter of 12.5 mm and length of 30 mm, were tested. A tubular specimen was considered for this program, but it was rejected because the small wall thickness required (less than 1 mm) would have likely introduced torsional buckling.

The biaxial fatigue tests were conducted on a closed-loop, servohydraulic tension-torsion load frame, with an axial load capacity of 445 kN and a torsional load capacity of 5000 N-m.

Strains were measured with a modified MTS model 632.85 biaxial extensometer with conical points. The modification involved strain-gauging existing flexure elements to measure torsional strains. All tests were initially started in strain control at 0.5 Hz or less. Prior to conducting the test, each specimen was cycled at low load levels to seat the extensometer and measure the axial and shear moduli of the specimen. Most tests were performed in strain control until failure; however, a limited number of tests were eventually switched to load control and run to failure at 2 Hz. This was only done if the stabilized cyclic deformation was linear elastic and there was no chance of introducing ratcheting by changing the mode of control.

The biaxial data obtained from this test program are summarized in Table 1, grouped according to type of test. The first test shown (156-11) is a fully reversed axial test. The next group of tests in the table (21-11 to 21-4) are torsion-only experiments at various R ratios. These tests were performed to ascertain whether mean shear stresses influence fatigue lives. It has been reported (e.g., Ref. [1]) that mean shear stresses have no effect on the fatigue behavior of metals. To determine if this observation holds true for Ti-6Al-4V, torsion tests were conducted at R ratios of -1, 0.1, and 0.5.

The next three tests (21-1 to 156-3) represent proportional, combined axial-torsion experiments (the principal stress directions remained fixed during the cycle). The remaining tests are non-proportional. Specimen 156-8 was loaded 90 degrees out-of-phase. This load path is often considered to be critical with regard to deformation and fatigue damage. The strain path for this test is shown in Figure 1(a). The other non-proportional tests were loaded in a triangle path, or in segments of this path. The triangle path, shown in Figure 1(b), is another out-of-phase approximation of service conditions. Specimens 156-2 and 21-2 were loaded in the full path, while the remaining specimens (156-6 to 156-7) were loaded in segments of this path, as defined in Figure 1(b). The Y+ or Y- notation indicate whether the static axial strain was positive or negative. Two tests (156-6 and 156-7) experienced control problems during testing, and were subsequently excluded from the analyses.

The stresses and strains reported in Table 1 represent stabilized, half-life values. While most specimens experienced only elastic strains during the loading, some specimens did incur small plastic strains with the first reversal. An elastic-plastic finite element analysis was performed by GEAE [2] for those tests; the resulting stresses obtained from the finite element analysis were used in this study, and are shown in Table 1. The elastic-plastic finite element analysis performed by GEAE assumed a Ramberg-Osgood correlation for the cyclic stress-strain curve, and used the following material properties: $E = 116 \text{ GPa}$, $K' = 854 \text{ MPa}$, $n' = 0.0149$ [2].

In addition to the biaxial data, over 100 data points from uniaxial fatigue tests were obtained from Pratt and Whitney, AlliedSignal, General Electric, and the Air Force Research Lab. These data included both strain-controlled (LCF) and load-controlled (HCF) tests, and covered a range of R ratios, including $R = -1, 0.1, 0.5, \text{ and } 0.8$. Test frequencies ranged from 0.33 Hz (LCF) to 1000 Hz (HCF). The uniaxial data used in this research are shown in Figure 2. These data were used to provide a baseline reference for comparison of the multiaxial fatigue models, and to further evaluate their capabilities with regard to mean stress effects.

MULTIAXIAL FATIGUE MODELS

A robust fatigue model must be capable of providing accurate life predictions, or allowable design stresses, under complex cyclic stress states, including non-proportional loading. Numerous multiaxial fatigue models have been proposed in the technical literature; however, the experimental verification of most of these models is fairly limited. In this study, 22 existing

models (or variations of such models) were evaluated by comparison of the uniaxial and biaxial HCF data for Ti-6Al-4V to the model predictions. The models selected for evaluation in this study can be classified into two categories: (1) equivalent (invariant) stress models and (2) critical plane models.

The equivalent stress models are essentially extensions of static yield criteria, such as the von Mises criterion, in which the cyclic multiaxial stresses are reduced to an equivalent cyclic scalar value. The equivalent stress history is then used in conjunction with uniaxial stress-life data, often with a mean stress modification, to predict the corresponding fatigue life. A difficulty arises with this type of procedure in the definition of a mean stress, which is vague within a multiaxial stress state. Due to their current usage, several equivalent stress-based models were evaluated in this study.

The critical plane models were developed in response to phenomenological observations of fatigue crack development, where it has been found that fatigue cracks often nucleate on critical planes. It is assumed that crack nucleation on a particular plane is a function of the normal and/or shear stresses and strains on that plane. Normal stresses (strains) are hypothesized to open the crack, reducing friction between the crack surfaces, while shear stresses (strains) induce dislocation movement along slip lines, causing nucleation and growth of cracks. As a result, critical plane damage parameters typically make use of some combination of normal and shear stresses or strains on a given plane.

The models considered in this study are briefly described below. The damage parameters are shown in equation form in Table 2.

Equivalent Stress Models

- 1) a) Goodman, b) Gerber, and c) Soderberg relations, with the stress amplitude and mean stress calculated using the definition of the von Mises equivalent stress [3].
- 2) a) Goodman, b) Gerber, and c) Soderberg relations, with the stress amplitude calculated using the definition of the von Mises equivalent stress, and the mean stress calculated using the definition of the hydrostatic stress [3].
- 3) Von Mises equivalent stress amplitude with multiaxiality factor correction [4]. The relationship between stress amplitude and fatigue life is modified by a multiaxiality factor, which is a function of the principal stresses.
- 4) Modified Manson-McKnight model [2]. A “pseudostress” range is defined in terms of the alternating stress components. A mean stress is defined in terms of the summation of stress components at different points in the loading cycle. An equivalent stress is then defined in terms of the maximum and alternating pseudostress range.

Critical Plane Models

- 5) Maximum normal strain amplitude with Morrow mean stress correction [5]. Fatigue life is a function of the max normal strain amplitude and the mean normal stress on the critical plane.
- 6) Maximum normal strain amplitude with Smith, Watson, and Topper (SWT) mean stress correction [6]. Fatigue life is a function of the maximum normal strain amplitude and the maximum normal stress on the critical plane.
- 7) Maximum normal stress amplitude with mean stress correction as predicted by the a) Goodman, b) Gerber, and c) Soderberg criteria. The same mean stress models as considered above in (1), but with the stress components calculated on the critical plane.
- 8) a) Goodman, b) Gerber, and c) Soderberg criteria modified for shear stresses. The same mean stress models as considered in (7), but modified to replace normal stress components with shear stress components.

- 9) Kandil, Brown, and Miller (KBM) parameter [7]. This parameter considers the maximum alternating shear strain to be the primary damage component on a plane, with the normal strain amplitude on this plane acting as a secondary damage component.
- 10) Findley parameter [8]. This parameter considers the maximum alternating shear stress to be the primary damage component on a plane, with the maximum normal stress on this plane (modified by an adjustable material parameter) acting as a secondary damage component.
- 11) McDiarmid parameter [9]. Similar to the Findley parameter, but with the adjustable material parameter defined as a constant in terms of the ultimate strength of the material and the fatigue strength in torsion.
- 12) Fatemi, Socie, and Kurath (FSK) parameter [10]. Considers the maximum alternating shear strain to be the primary damage component on a plane, with the maximum normal stress on this plane (modified by an adjustable parameter) acting as a secondary damage component.
- 13) Chu, Conle, and Bonnen (CCB) parameter [11]. An energy-based parameter, defined by multiplying the shear and normal strain amplitudes on a plane with the corresponding shear and normal maximum stresses on that plane, and then adding the terms together. This model was also modified by multiplying one of the terms by an adjustable parameter.
- 14) Glinka, Wang, and Plumtree (GWP) parameter [12]. Another energy-based parameter, defined as the product of the shear strain amplitude on a plane, the shear stress amplitude on that plane, and a term involving the maximum shear and normal stresses on that plane.

IMPLEMENTATION

The multiaxial fatigue models were evaluated based on their ability to correlate both the uniaxial and multiaxial fatigue data. This was accomplished by calculating the “damage parameter” for each model from the stress and strain values associated with each of the experimental tests. The calculated damage parameters were then plotted vs. the corresponding experimental fatigue lives. An effective fatigue model (damage parameter) can be considered to be one that essentially “collapses” all the data (i.e., uniaxial data at different R ratios and multiaxial data, both proportional and non-proportional loading) into a narrow band that can be represented with small error by a single curve.

In the presence of non-proportional or out-of-phase loading, the calculation of the damage parameters requires a “time-stepping” or incremental procedure, since the individual stress and strain components do not reach maximum values at the same time (i.e., the principal stress directions rotate during the cycle). In this study, each loading cycle was discretized into 20 to 30 increments. At each increment, the input stress and strain components were specified. For the equivalent stress models, the principal stresses were then calculated at these increments, which were subsequently used to calculate the von Mises and hydrostatic stresses at each point. The maximum and minimum values were identified, and the alternating and mean equivalent stresses were then determined in the conventional manner. Finally, the damage parameters were calculated from the alternating and mean equivalent stresses.

The critical plane models required implementation of stress and strain rotation procedures to identify the critical plane. The damage parameters for each of the critical plane models were determined on each plane, and the critical plane was identified as the plane with the maximum value of the damage parameter. Since all stress states were uniaxial or biaxial, a two-dimensional transformation was used to calculate the normal and shear stress and strain components on planes at 2° increments from 0° to 90°, rotated about a line perpendicular to the surface of the specimen. This procedure is shown schematically in Figure 3. These components

were calculated at each increment (again using 20 to 30 increments for the loading cycle) on each plane. The maximum and minimum values of the stress and strain components were determined on each plane, from which the alternating and mean components were calculated. These components were then used to calculate the damage parameters, as defined in Table 2. Note that, for the uniaxial and proportional biaxial tests, the full incremental procedure was not necessary. Since all components reached maximum and minimum values at the same time, the calculations were only performed at the reversal points of the loading cycle.

MODEL COMPARISONS

A preliminary assessment of the models listed in Table 2 was made by evaluating their ability to correlate (collapse) the uniaxial and biaxial fatigue data. Ideally, the data should collapse into a single curve that coincides with the uniaxial, fully-reversed ($R = -1$) fatigue curve, which is often considered to be the baseline fatigue behavior. This characteristic is desirable because it would allow for the calculation of all necessary fatigue parameters from a limited set of data. For this reason, the preliminary assessment of the multiaxial fatigue models was performed by comparison of the damage parameter vs. life data, obtained from each model, to the fully-reversed, uniaxial fatigue curve.

Due to space limitations, the graphical results of the preliminary assessment are not shown here. However, a broad qualitative summary of the results is provided in Table 2. Three measures of the adequacy of each model at correlating the fatigue data are shown. In the third column, the ability of each model to correlate the uniaxial data (i.e., collapse the data for each R ratio onto the fully-reversed curve) is rated using a simple good/fair/poor scale. The last two columns summarize the ability of the models to correlate the biaxial data to the baseline curve, in terms of two indicators. The first indicator (mean) gives a measure of how well the data were centered about the baseline curve; i.e., if the data were roughly centered about the curve, or if the data tended to fall below (low) or above (high) the baseline curve. This measure gives an indication of whether the model tends to be conservative (high) or non-conservative (low) when predicting the damage or fatigue life under a multiaxial state of stress. The last indicator (scatter) provides a qualitative measure of the degree of scatter or spread in the biaxial data about the mean. A desirable multiaxial fatigue model is one that would provide a good correlation of all uniaxial data about the $R = -1$ curve, and also center the biaxial data about this curve with a low degree of scatter.

It is evident from the results shown in Table 2 that the critical plane models, in general, were more successful at correlating the fatigue data than the equivalent stress models. Of the equivalent stress models, only the modified Manson-McKnight model (#4) provided a good correlation of the uniaxial data, and correlated the biaxial data with a moderate amount of scatter. Of the critical plane models, several demonstrated some desirable characteristics, most notably the SWT (6), Findley (10), FSK (12), and CCB (13) models. Note that the Findley and FSK parameters both include an adjustable material constant, k . In the preliminary evaluation, values of $k = 0.45$ (Findley) and 1.0 (FSK) were used. Although several models appeared to be promising, none in the present form demonstrated ideal characteristics (i.e., good, centered, and low in the last three columns of Table 2).

After consideration of the results shown in Table 2, six of the models were chosen for more detailed study. These models were selected due to their good agreement with the experimental data, or because of their familiarity or preference by other members of the HCF program. The models selected for more detailed evaluation were the modified Manson-McKnight (4), SWT

(6), Goodman critical plane (based on normal stresses, 7a), Findley (10), FSK (12), and CCB (13) models. The same general procedures were followed in the implementation of the models. However, a more thorough evaluation of the influence of the empirical “k” factors (for the Findley and FSK models) was performed, and the effect of the curve fit to the uniaxial data was evaluated. Specifically, a curve fit to the uniaxial data was generated that included all R ratios, rather than just the fully-reversed (R = -1) data. This was done in order to produce a better overall representation of both the uniaxial and biaxial data.

For each of the selected models, plots of the damage parameter (calculated from the applied stress state) vs. experimental fatigue life are shown in Figures 4 through 9. Two plots are shown for each model: the left plot shows the uniaxial data, separated by R ratio, while the right plot shows the biaxial data, separated by type of test. The curves in all of the plots represent the best fit to the uniaxial data, utilizing a two-parameter power law relationship between damage parameter and fatigue life. This equation has the general form

$$DP = A(N_f)^b + C(N_f)^d$$

where DP is the damage parameter (as shown in Table 2), N_f is the fatigue life, and A, b, C, and d are curve-fitting parameters. These parameters were adjusted so that the resulting curve provided a good representation of the uniaxial data. The notation used in this equation indicates that the conventional strain-life constants were not utilized in this analysis.

As previously noted, the Findley and FSK parameters both include an empirical “k” factor. This factor is assumed to be a material parameter, which must generally be determined by evaluation of both uniaxial and multiaxial data. In this study, the influence of the k factor was thoroughly investigated for each model. For the Findley parameter, k was varied from 0.15 to 0.55, in increments of 0.05. For the FSK parameter, k was varied from 0.5 to 8.0 in increments of 0.1. The optimal k values, which provided the best overall correlation of both the uniaxial and biaxial data, were found to be 0.35 for the Findley model and 6.0 for the FSK model.

As is evident from Figures 4 through 9, most of the models were fairly successful at correlating the uniaxial data over the various R ratios. For the Findley, FSK, modified Manson-McKnight, SWT, and CCB models, the correlation can be considered to be very good, in that the data collapse into a fairly narrow band. There appears to be a bit more scatter with the Goodman model, primarily at the higher R ratios. Although all the selected models provided an adequate correlation of the uniaxial data, there were significant differences in their abilities to correlate the biaxial data. The Findley parameter (Fig. 7) and FSK parameter (Fig. 8) provide the best overall correlation of the biaxial data, in that the uniaxial curves roughly pass through the center of the data and the scatter around the curves is relatively small (the results shown in these figures would be indicative of a “good” correlation of uniaxial data, and a “centered” mean with “low” scatter in correlating the biaxial data, as indicated in Table 2). The FSK model does appear to suffer from some “layering” of the uniaxial data by R ratio, but the overall correlation can be considered to be quite good. The uniaxial curve for the modified Manson-McKnight model (Fig. 4) is fairly well centered about the biaxial data, but there is more scatter around the curve (indicative of “moderate” scatter for the biaxial data in Table 2). For the SWT and Goodman models (Figs. 5 and 6), the uniaxial curves pass above the biaxial data, meaning the biaxial stress states are more damaging than the models would predict (“low” mean with “low” to “moderate” scatter in Table 2). As both of these models are normal stress-based models, this would indicate that a shear-cracking mode may be dominant during nucleation of fatigue cracks in this material. Finally, the uniaxial curve for the CCB model (Fig. 9) passes below the biaxial data, meaning the

damage predictions by this model are somewhat conservative (“high” mean in Table 2).

Based on the good results obtained from the Findley and FSK parameters, which both utilized the adjustable “k” factor as a multiplier on the normal stress term, a modification of the CCB model was also implemented. This modification involved multiplying the second term in the damage parameter ($\epsilon_a \sigma_{\max}$) by an adjustable factor, k. For this model, k was varied from 0.5 to 4.0 in increments of 0.1. The optimal k value, which provided the best correlation of both the uniaxial and biaxial data, was found to be 2.7. The results of this modification are shown in Figure 10. It can be seen that this modification significantly improved the damage predictions for both the uniaxial and biaxial tests.

SUMMARY AND CONCLUSIONS

Although several models adequately correlated the uniaxial data, few models successfully predicted the relationship between damage and fatigue life for the biaxial data. This was particularly evident when the loading state was non-proportional or out-of-phase. Of the equivalent (invariant) stress models considered here, the modified Manson-McKnight model clearly provided the best overall correlation of both the uniaxial and biaxial data. However, while the results for the uniaxial data were quite good, the correlation of the biaxial data was only fair. Conversely, several critical plane models provided very good predictions for both the uniaxial and biaxial data, the most notable being the Findley, FSK, and modified CCB models. Based on these results, it appears that a shear-cracking mode is likely the predominant damage mode during crack nucleation for this material. This is further supported by the results from some normal-stress based damage parameters, such as the SWT parameter. This parameter correlated the uniaxial data quite well, but resulted in a significant mean offset between predicted and experimental biaxial data.

It should be noted that the accuracy of the Findley, FSK, and modified CCB models was enhanced by the fact that all damage parameters included an adjustable material parameter (k factor). While an adjustable parameter is desirable due to the potential improvement in predictions (as found here), it also generally necessitates more experimental fatigue data to determine its value.

It is also worth noting that, based on the results shown in Table 2, mean shear stresses do appear to have some effect on the fatigue life of Ti-6Al-4V. This is evidenced by the fact that, at equivalent shear stress amplitudes (e.g., specimens 156-10 and 156-5), the presence of a mean shear stress (156-5) reduced the fatigue life relative to the fully-reversed case (156-10).

ACKNOWLEDGEMENT

This work was supported under Air Force Contract No. F49620-99-C-0007, Advanced High Cycle Fatigue Life Assurance Methodologies, with Mr. Joseph G. Burns, AFRL/MLLN, Project Monitor. The contract is being administrated through the University of Dayton Research Institute under subcontract RSC99013 with North Dakota State University.

REFERENCES

- 1) Sines, G. and Ohgi, G., “Fatigue Criteria under Combined Stresses or Strains,” *ASME Journal of Engineering Materials and Technology*, Vol. 103, 1981, pp. 82-90.
- 2) Slavik, D. and Kurath, P., “Fatigue Crack Initiation Modeling in Ti-6Al-4V for Smooth and Notched Specimens under Complex Stress States,” *Fifth National Turbine Engine HCF Conference*, 2000.

- 3) Shigley, J. E. and Mischke, C. R., *Mechanical Engineering Design*, McGraw-Hill, New York, 1989.
- 4) Manson, S. S. and Jung, K., "Progress in the Development of a Three-Dimensional Fatigue Theory Based on the Multiaxiality Factor," *Material Durability/Life Prediction Modeling: Materials for the 21st Century*, PVP-Vol. 290, ASME, 1994, pp. 85-93.
- 5) Morrow, J., *Fatigue Design Handbook*, SAE AE-6, J. A. Graham, Ed., Society of Automotive Engineers, 1968, pp. 17-58.
- 6) Smith, R. N., Watson, P., and Topper, T. H., "A Stress-Strain Function for the Fatigue of Metals," *Journal of Materials*, JMLSA, Vol. 5., 1970, pp. 767-778.
- 7) Kandil, F. A., Brown, M. W., and Miller, K. J., "Biaxial Low-Cycle Fatigue Fracture of 316 Stainless Steel at Elevated Temperatures," Book 280, The Metals Society, London, 1982, pp. 203-210.
- 8) Findley, W. N., "Fatigue of Metals Under Combinations of Stresses," *Transactions*, ASME, Vol. 79, 1957, pp. 1337-1348.
- 9) McDiarmid, D. L., "A General Criterion for High Cycle Multiaxial Fatigue Failure," *Fatigue Fract. Engng. Mater. Struct.*, Vol. 14, No. 4, 1991, pp. 429-453.
- 10) Fatemi, A. and Kurath, P., "Multiaxial Fatigue Life Predictions Under the Influence of Mean Stresses," *ASME Journal of Engineering Materials and Technology*, Vol. 110, 1988, pp. 380-388.
- 11) Chu, C. C., Conle, F. A., and Bonnen, J. J. F., "Multiaxial Stress-Strain Modeling and Fatigue Life Prediction of SAE Axle Shafts," *Advances in Multiaxial Fatigue, ASTM STP 1191*, D. L. McDowell and R. Ellis, Eds., American Society for Testing and Materials, Philadelphia, 1993, pp. 37-54.
- 12) Glinka, G., Wang, G., and Plumtree, A., "Mean Stress Effects in Multiaxial Fatigue," *Fatigue Fract. Engng. Mater. Struct.*, Vol. 18, No. 7/8, 1995, pp. 755-764.

TABLES AND FIGURES

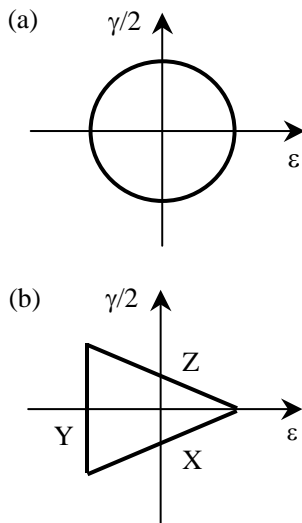


Figure 1. Non-proportional strain paths: (a) 90° out-of-phase (O-P) path and (b) triangle path.

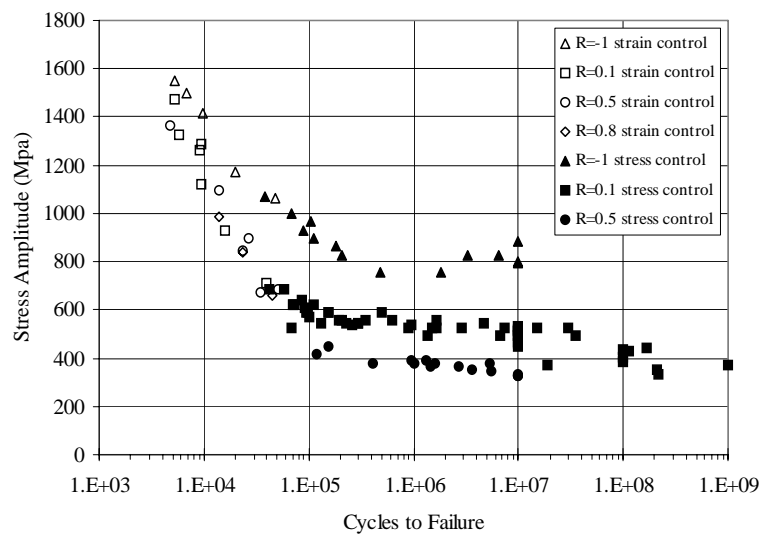


Figure 2. Uniaxial fatigue data.

Table 1. Biaxial Fatigue Data

Spec. ID	ϵ_{\max} (%)	ϵ_{\min} (%)	γ_{\max} (%)	γ_{\min} (%)	σ_{\max} (MPa)	σ_{\min} (MPa)	τ_{\max} (MPa)	τ_{\min} (MPa)	N_f (cycles)	Test Conditions
156-11	0.756	-0.751	-	-	821	-843	0	0	6,200	Axial, R=-1
21-11	-	-	0.866	-0.868	0	0	375.8	-375.5	72,141	Torsion, R=-1
21-6	-	-	0.614	-0.610	0	0	266.1	-264.7	241,250	Torsion, R=-1
156-10	-	-	0.559	-0.563	0	0	242.7	-244.1	961,806	Torsion, R=-1
21-7	-	-	1.81	0.166	0	0	454	-252	30,007	Torsion, R=0.1
156-5	-	-	1.21	0.090	0	0	443	-38.6	150,293	Torsion, R=0.1
156-4	-	-	1.36	0.150	0	0	448	-71.7	151,598	Torsion, R=0.1
156-1	-	-	0.958	0.086	0	0	415.7	47.2	814,753	Torsion, R=0.1
21-4	-	-	1.96	0.815	0	0	455.7	-36.5	141,229	Torsion, R=0.5
21-1	0.312	-0.312	0.416	-0.418	365.4	-365.4	180.6	-181.3	67,965	Proportional, R=-1
156-9	0.462	0.049	0.616	0.055	540.6	57.2	267	24.1	60,514	Proportional, R=0.1
156-3	0.464	0.048	0.621	0.055	543.3	55.8	269	24.1	87,920	Proportional, R=0.1
156-8	0.303	-0.302	0.406	-0.409	352.5	-350.9	175.2	-176.5	111,783	90° O-P, R=-1
156-2	0.362	-0.373	0.471	-0.476	424	-436	204	-204	38,355	Triangle path
21-2	0.364	-0.372	0.471	-0.477	426.1	-435.8	204.1	-206.8	43,009	Triangle path
156-6	0.363	-0.361	0.476	0.004	426	-435	209	5.6	>19,864	Z leg of triangle*
21-9	0.364	-0.364	0.475	0.004	426	-426	206.2	2.1	71,358	Z leg of triangle
21-5	0.365	-0.363	-0.005	-0.475	427.5	-424.7	-2.1	-206.2	79,367	X leg of triangle
21-8	0.091	0.089	0.666	-0.665	106.2	104.8	288.9	-288.2	72,124	Y+ leg of triangle
21-3	0.090	0.089	0.666	-0.666	105.5	104.1	288.9	-288.9	73,728	Y+ leg of triangle
21-10	-0.089	-0.091	0.665	-0.664	-104.1	-106.9	288.9	-288.9	329,058	Y- leg of triangle
156-7	-0.089	-0.091	0.663	-0.667	110	-114	292	-294	>24,576	Y-leg of triangle*

* Control problem during test (invalid)

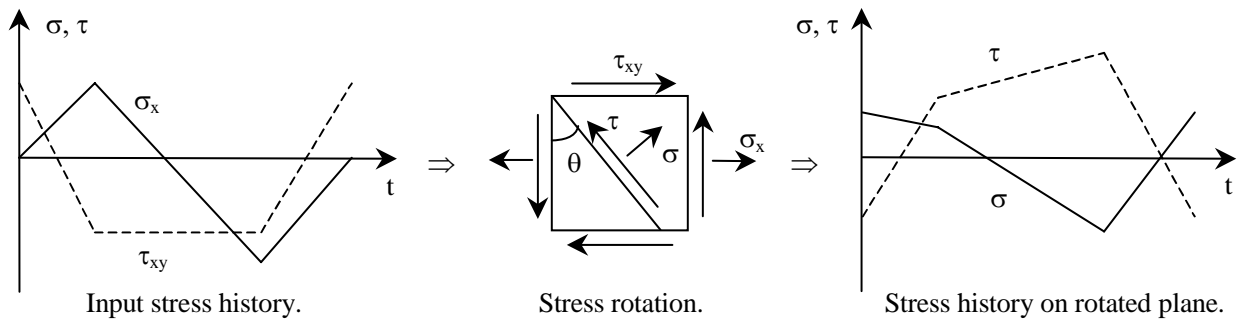


Figure 3. Implementation of critical plane models.

Table 2. Preliminary Model Comparisons.

Model		Damage Parameter DP = f(N _f)	Correlation of Uniaxial Data	Correlation of Biaxial Data Mean Scatter	
Equivalent Stress Models	1a) Goodman (v. Mises)	$\sigma_{a,VM} \left[1 - (\sigma_{m,VM}/\sigma_{ut}) \right]^{-1}$	Fair	Centered	High
	1b) Gerber (v. Mises)	$\sigma_{a,VM} \left[1 - (\sigma_{m,VM}/\sigma_{ut})^2 \right]^{-1}$	Poor	Centered	High
	1c) Soderberg (v. Mises)	$\sigma_{a,VM} \left[1 - (\sigma_{m,VM}/\sigma_y) \right]^{-1}$	Fair	Centered	High
	2a) Goodman (hydro.)	$\sigma_{a,VM} \left[1 - (\sigma_{m,H}/\sigma_{ut}) \right]^{-1}$	Poor	Centered	High
	2b) Gerber (hydro.)	$\sigma_{a,VM} \left[1 - (\sigma_{m,H}/\sigma_{ut})^2 \right]^{-1}$	Poor	Centered	High
	2c) Soderberg (hydro.)	$\sigma_{a,VM} \left[1 - (\sigma_{m,VM}/\sigma_y) \right]^{-1}$	Poor	Centered	High
	3) Multiaxiality factor	$\sigma_{a,VM} = f(N_f, MF)$	Poor	Centered	High
	4) Manson-McKnight	$\sigma_{a,psu}^{(1-w)} \sigma_{max}^w$	Good	Centered	Moderate
Critical Plane Models	5) Morrow	$\epsilon_a = f(N_f, \sigma_m)$	Fair	Centered	Moderate
	6) Smith-Watson-Topper	$\epsilon_a \sigma_{max}$	Good	Low	Low
	7a) Goodman (normal)	$\sigma_a \left[1 - (\sigma_m/\sigma_{ut}) \right]^{-1}$	Fair	Low	Moderate
	7b) Gerber (normal)	$\sigma_a \left[1 - (\sigma_m/\sigma_{ut})^2 \right]^{-1}$	Poor	Low	Moderate
	7c) Soderberg (normal)	$\sigma_a \left[1 - (\sigma_m/\sigma_y) \right]^{-1}$	Fair	Low	Moderate
	8a) Goodman (shear)	$\tau_a \left[1 - (\tau_m/\tau_{ut}) \right]^{-1}$	Fair	Centered	High
	8b) Gerber (shear)	$\tau_a \left[1 - (\tau_m/\tau_{ut})^2 \right]^{-1}$	Poor	Centered	High
	8c) Soderberg (shear)	$\tau_a \left[1 - (\tau_m/\tau_y) \right]^{-1}$	Fair	Centered	High
	9) Kandil-Brown-Miller	$\gamma_a + \epsilon_a$	Poor	Centered	Moderate
	10) Findley	$\tau_a + k\sigma_{max} \quad (k = 0.45)$	Fair	Centered	Low
	11) McDiarmid	$\tau_a \left[1 - (\sigma_{max}/2\sigma_{ut}) \right]^{-1}$	Poor	Centered	Moderate
	12) Fatemi-Socie-Kurath	$\gamma_a \left[1 + k(\sigma_{max}/\sigma_y) \right] \quad (k = 1)$	Fair	Centered	Moderate
	13) Chu-Conle-Bonnen	$2\gamma_a \tau_{max} + \epsilon_a \sigma_{max}$	Good	High	Moderate
	14) Glinka-Wang-Plum.	$\gamma_a \tau_a \left[(1 - \tau_{mx}/\tau'_f)^{-1} + (1 - \sigma_{mx}/\sigma'_f)^{-1} \right]$	Poor	Centered	High

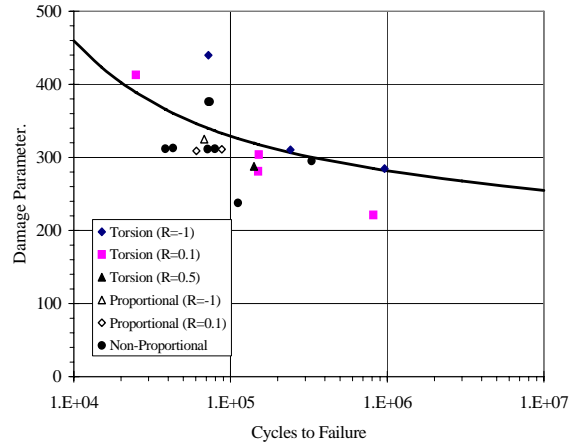
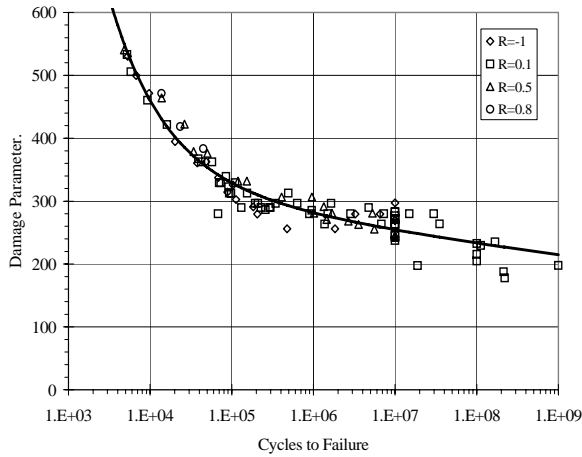


Figure 4. Modified Manson-McKnight model (model 4).

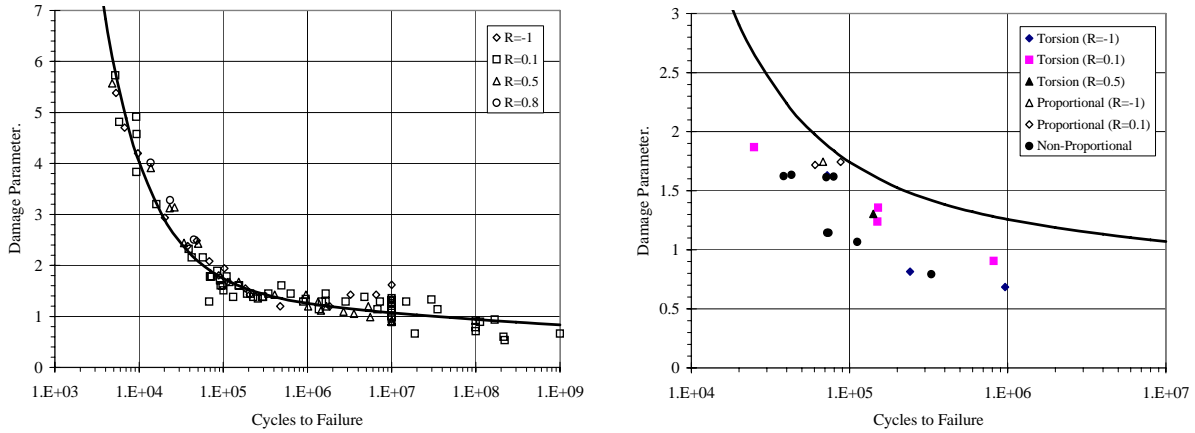


Figure 5. Smith, Watson, and Topper (SWT) model (model 6).

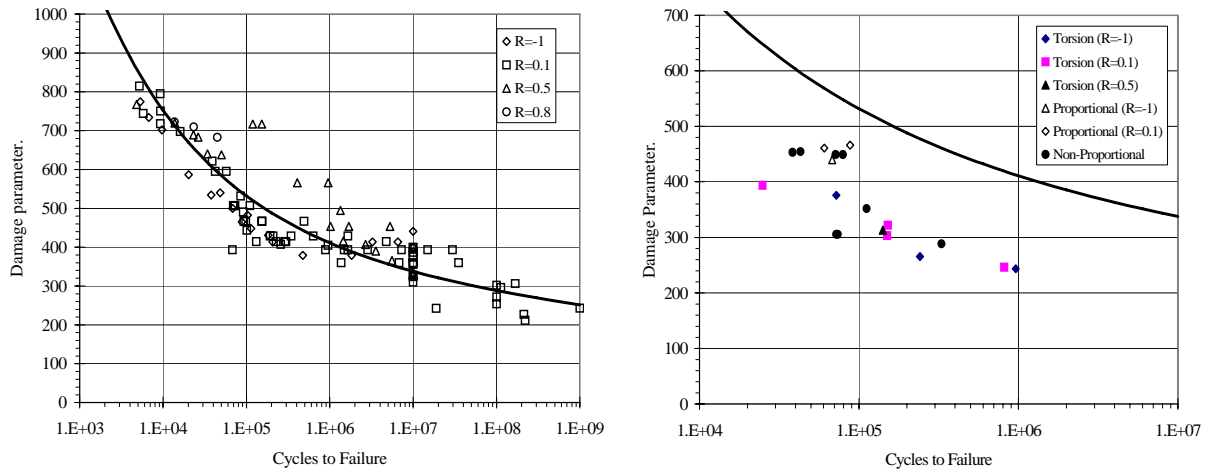


Figure 6. Goodman critical plane model (normal stress) (model 7(a)).

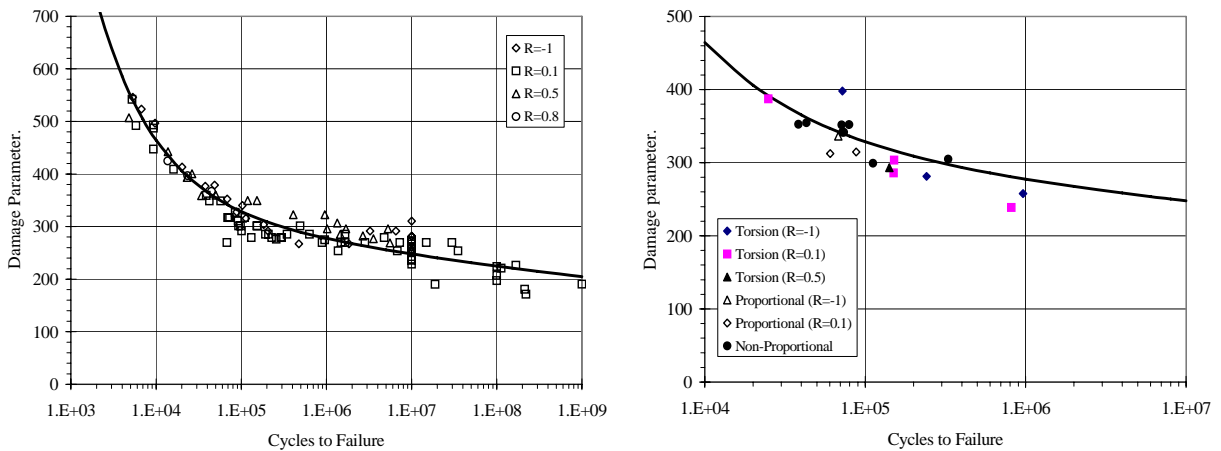


Figure 7. Findley model, with $k = 0.35$ (model 10).

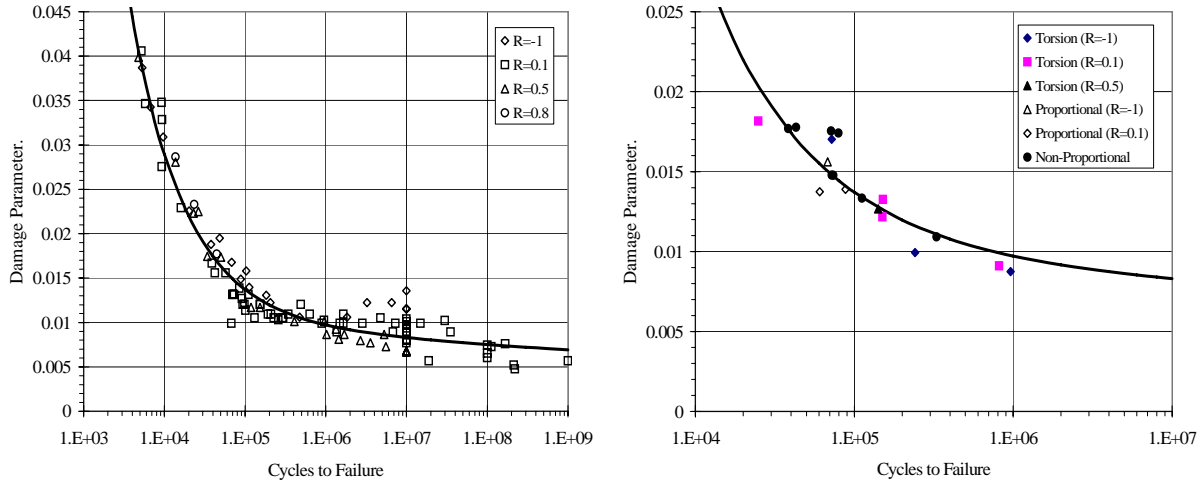


Figure 8. Fatemi, Socie, and Kurath (FSK) model, with $k = 6.0$ (model 12).

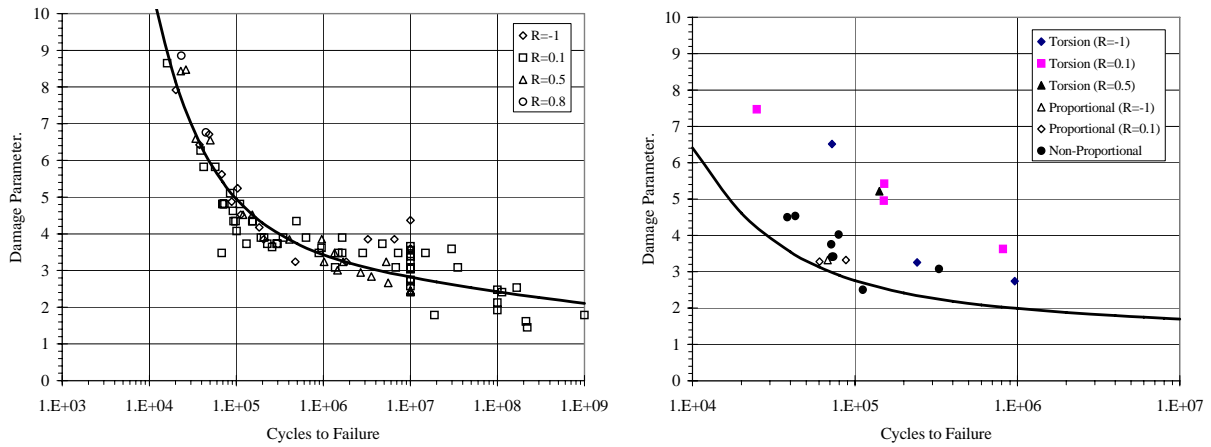


Figure 9. Chu, Conle, and Bonnen (CCB) model (model 13).

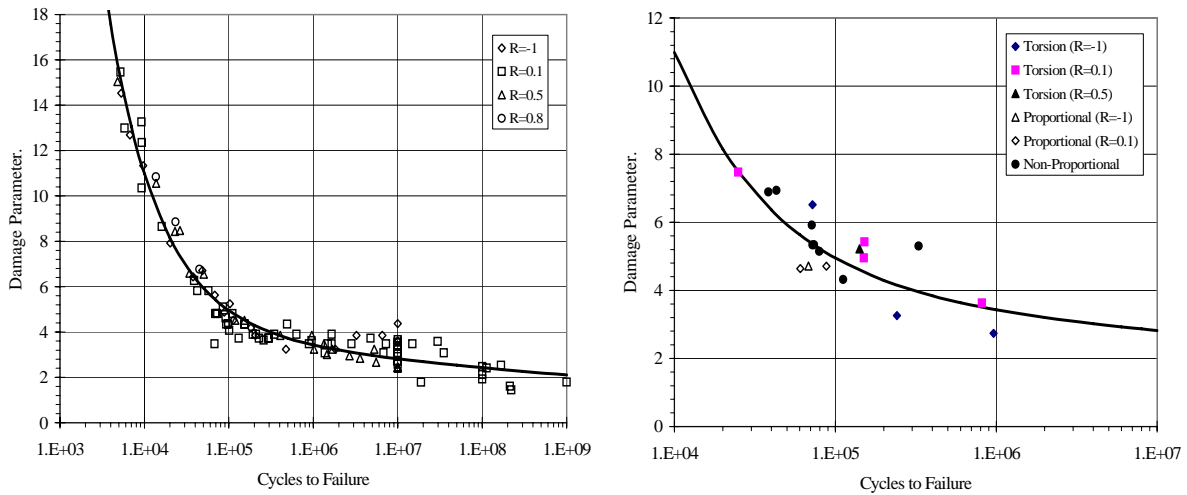


Figure 10. Modified Chu, Conle, and Bonnen model, with $k = 2.7$ (model 13).